Supplemental Materials

for

Postsynthesis of High Silica Beta by Cannibalistic Dealumination of OSDA-Free Beta and Its Catalytic Applications

Peng Luo, Hao Xu*, Teng Xue, Jingang Jiang, Haihong Wu, Mingyuan He, Peng Wu*

Shanghai Key Laboratory of Green Chemistry and Chemical Processes, School of Chemistry and Molecular Engineering, East China Normal University, North Zhongshan Road 3663, Shanghai 200062, China

Tel: +86-21-6223-2292

Fax: +86-21-6223-2292

E-mail address: hxu@chem.ecnu.edu.cn (H. Xu); pwu@chem.ecnu.edu.cn (P. Wu)

Experimental Section

Synthesis of pristine OSDA-free Al-rich Beta zeolite. The pristine Al-rich Beta was synthesized *via* a seeding method without using any OSDA according to the literature [1]. Typically, 119.2 g $Al_2(SO_4)_3\cdot 18H_2O$ and 28.4 g NaOH and 423.3 g water glass (SiO_2, 27.10 wt%; Na_2O, 8.39 wt%) were firstly dissolved in 449.6 g H_2O in sequence under vigorous stirring. Subsequently, 11.4 g industrial Beta (Si/Al=11.4) as seeds (10 wt.%) was added to give a molar composition of 1.0 SiO_2 : 0.1 Al_2O_3 : 0.22 Na_2O : 20 H_2O. The mixture was homogenized under stirring for 2 h, and then transferred into a 1 L Teflon-lined stainless steel autoclave and heated at 393 K for 5 days. The product obtained was filtered, washed with deionized water several times, dried overnight at 373 K, and then calcined at 823 K for 6 h, and the prepared product is denoted as Na Beta. It was converted into ammonium form *via* ion-exchange with 1 M ammonium chloride solution at 353 K for 2 h, then dried at 373 K. This treatment was repeated for three times and followed by calcination at 823 K for 6 h to give the proton type Beta, denoted as PR Beta.

Relative crystallinity and yield calculation method. The relative crystallinity was calculated using the equation (RC=CS/CR) based on the XRD patterns and the Na Beta as reference, where RC was the relative crystallinity, CR was the sum of the peak intensity of 2θ=7.6° and 22.6° of reference, CS was the sum of the peak intensity of 2θ=7.6° and 22.6° of CD Beta samples. The solid product yield was calculated using the equation (Y=MS/MR) based on the mass, where Y was the yield, MR was the sum mass of Beta and $Al_2(SO_4)_3$ in the initial aqueous solution, MS was the mass of solid product (including Beta and natroalunite phase) recovered from the solution after the $Al_2(SO_4)_3$-induced dealumination process.

Hydrothermal stability test

For hydrothermal stability test, various Beta zeolites were put into a quartz tube with an inner diameter of 8 mm with a continuous 20 mL min^{-1} N_2 flow until the temperature reached 1053 K. Then water was fed into the reactor at a rate of 1 mL h^{-1} at 1053 K for 2 h under the same nitrogen flow. The treated samples were characterized by XRD and FT-IR analyses.

Chemical reactions involved in the cannibalistic dealumination (CD) process

The Gibbs free energy of Beta zeolites (($H_2O\bullet Al_2O_3)_{n1}(Na_2O\bullet Al_2O_3)_{n2}(SiO_2)_{n3}$) are calculated according to the equation: ΔG^0zeolite = n1 ΔG^0 zeolite-H_2O + n1 ΔG^0 zeolite-Al_2O_3 + n2 ΔG^0 zeolite-

Na$_2$O•Al$_2$O$_3$ + n3 ΔG^0 zeolite-SiO$_2$ [2-3]. ΔG^0zeolite-H$_2$O = -237.2 kJ mol^{-1}, ΔG^0 zeolite-Al$_2$O$_3$ = -1690.9 kJ mol^{-1}, ΔG^0 zeolite-Na$_2$O•Al$_2$O$_3$ = -2273.1 kJ mol^{-1}, ΔG^0 zeolite-SiO$_2$ = -855.9 kJ mol^{-1}.

The Gibbs free energy of Al$_2$(SO$_4$)$_3$ is calculated on the physical parameters calculation software (ap 1700), ΔG^0Al$_2$(SO$_4$)$_3$ = -3098.5 kJ mol^{-1}. The Gibbs free energy of other materials are as following: ΔG^0H$_2$O$^{(423\ K,\ 0.38MPa)}$ = –217.3 kJ mol^{-1}, ΔG^0Na$_2$SO$_4$ = -1270.2 kJ mol^{-1}, ΔG^0NaAl$_3$(SO$_4$)$_2$(OH)$_6$ = -4622.4 kJ mol^{-1}, ΔG^0NaOH = -379.5 kJ mol^{-1}, ΔG^0NaAlO$_2$= -1069.2 kJ mol^{-1} [4-5].

Table S1 Element and mass balance.

Sample	No.	Phase	Total (g)	Si (g)	Al (g)	Na (g)	S (g)	H (g)	O (g)
Feeding	1	Na Beta	1000[a]	354[b]	79[b]	68[b]	< 1	-	499[f]
Materials	2	Al$_2$(SO$_4$)$_3$	357[a]	< 1	57	< 1	100	-	200[f]
(dry base)	3	Sum	1357	354	136	68	100	-	699
	4	Beta zeolite	860[a]	354[b]	45[c]	2[d]	-	1[f]	458[f]
CD Beta-7.6	5	Natroalunite	448[a]	-	91[e]	26[e]	72	7[f]	252[f]
	6	Sum (solid)	1308	354[b]	136[b]	28[b]	72	8	710
	7	Na$_2$SO$_4$	124	<1	<1	40	28	-	56[f]
DeAl Bata	8	Beta zeolite	876[a]	354	45[b]	18[b]	<1	1[f]	458[f]
-7.6	9	NaOH	275[a]	-	-	158	-	7[f]	110[f]
	10	Sum (Solid)	1151	354[b]	45	176	-	8	568

[a] The weight of solid was the sum amount of Si, Al, Na, S, H and O.

[b] The amounts were determined by ICP analysis.

[c] The weight of Al element (No. 4) was obtained according to the framework Si/Al ratio for Beta zeolite (Si/Al = 7.6) and the Si amount.

[d] The weight of Na element in CD Beta (No. 4) was calculated according to the molecular formula of Beta after CD treatment.

[e] The weight of Al and Na elements in Natroalunite (No. 5) were obtained as No. 6 - No. 4.

[f] The weight of H and O elements were calculated according to the molecular formula of zeolite, natroalunite, NaOH and Na$_2$SO$_4$.

Nos. 1 and 2 are the initial feeding materials, consisting of Na Beta and Al$_2$(SO$_4$)$_3$, and we take 1000 g Na Beta as the initial feeding quantity for convenience. CD Beta consists of two phases of Beta and natroalunite (Nos. 4 and 5), containing Si, Al, Na, S, H, O elements. In the CD process with Al$_2$(SO$_4$)$_3$, 43% Al of Na Beta was extracted from zeolite skeleton, and the framework Si/Al ratio increased from 4.3 to 7.6. Most aluminum species existed in the natroalunite phase. Meanwhile, sodium sulfate was generated (No. 7), 97% Na ions were extracted from the zeolite, and the Si/Na ratio increased from 4.3 to 145, that is, the zeolite phase in CD Beta was almost proton type Beta zeolite. Among them, 37.3% Na ions were involved in the dealumination reaction (equation 2), and 59.7% sodium was involved in the by-reaction (equation 3). When the concentration of Al$_2$(SO$_4$)$_3$ was increased to 1.12 mol L^{-1}, more percentage of Na ions were reacted in the dealumination reaction (55.2%), and more Al species was removed from the Na Beta, resulting in the DeAl Beta with framework Si/Al ratio of 12. After washing with low concentration of NaOH, the natroalunite phase was completely removed from CD Beta, leaving a pure Beta phase with a higher Si/Al ratio of 7.6. Overall, we calculated the element and mass balance of the whole process based on the experimental data, and Al$_2$(SO$_4$)$_3$ was almost 100% involved in the reaction.
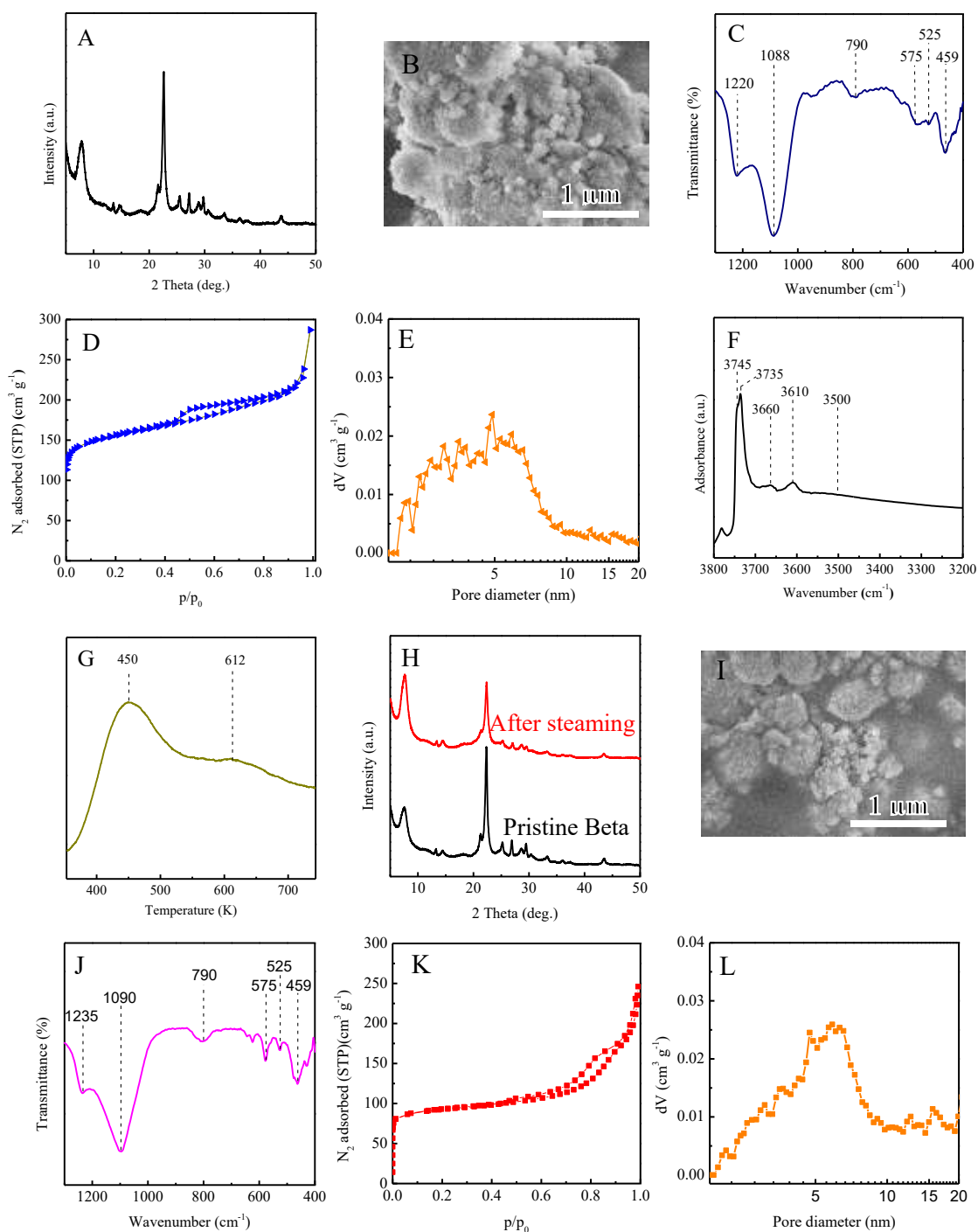
Fig. S1 Basic physicochemical properties of industrial Beta zeolite: (A) XRD pattern, (B) SEM image, (C) FT-IR spectrum, (D) N$_2$ sorption isotherm, (E) pore size distribution curve, (F) FT-IR spectrum in the hydroxyl region (in proton form), (G) NH$_3$-TPD profile. Physicochemical properties of industrial Beta zeolite after hydrothermal stability test: (H) XRD pattern, (I) SEM image, (J) FT-IR spectrum, (K) N$_2$ sorption isotherm and (L) pore size distribution curve.

The X-ray diffraction (XRD) pattern of industrial Beta (Si/Al=11.4) displayed well-resolved diffraction peaks characteristic of the BEA* topology with a relatively high crystallinity (Fig. S1A). The industrial Beta consisted of nanoparticles (Fig. S1B). In Fig. S1C, a band about 1088 cm^{-1} with a shoulder band at about 1220 cm^{-1} arising from asymmetric T-O-T stretching vibrations, a band around 790 cm^{-1} assigned to symmetric T–O–T stretching and characteristic skeletal vibrations at 575, 525 and 459 cm^{-1} belong to the BEA* topology [6-9]. Fig. S1D displayed nitrogen sorption isotherm of industrial Beta, giving total surface area and micropore volume of about 577 $cm^2\ g^{-1}$ and 0.18 $cm^3\ g^{-1}$, respectively. In addition, the external surface area of 144 $cm^2\ g^{-1}$ and mesopore volume of 0.27 $cm^3\ g^{-1}$, might be related to the aggregation of nanoparticles. Furthermore, the mesopores with size of 2 - 10 nm were observed in the pore size distribution of the industrial Beta (Fig. S1E). Fig. S1F showed the IR spectra in the region of hydroxyl stretching vibration, giving five peaks with the wavenumber centered at 3500, 3610, 3660, 3735, and 3745 cm^{-1}, which attributed to the hydrogen bonded silanol nests, hydroxyl related to framework Al, hydroxyl related to extra framework Al, non-acidic hydroxyl groups at defect sides inside the crystals, and the terminal silanols on the external surface [10-14]. Fig. S1G showed NH_3-TPD curve of industrial Beta, showing two desorption peaks centered at about 450 K and 612 K, which were attributed to weak and strong acid sites. Fig. S1H-L showed XRD, SEM, FT-IR, N_2 sorption isotherm and pore size distribution curve after hydrothermal stability test of the industrial Beta. The crystallinity of the pristine industrial Beta sample was assumed to be 100% and the relative crystallinity slightly decreased to 89.6% based on the sum of the peak area of $2\theta=7.6°$ and 22.6°in XRD patterns. It could be seen from SEM image that its morphology does not change after hydrothermal treatment. FT-IR spectra also demonstrated the preservation of the BEA* topology. However, N_2 sorption isotherm showed an obvious decrease of the microporous surface area and volume (159 $cm^2\ g^{-1}$ and 0.10 $cm^3\ g^{-1}$) after hydrothermal treatment (Table S2), lower than the fresh industrial Beta (433 $cm^2\ g^{-1}$ and 0.18 $cm^3\ g^{-1}$, respectively). The pore size distribution curve of industrial Beta determined by NLDFT analysis after hydrothermal treatment revealed a smaller amount of mesopores in the range of 2 - 10 nm than the parent industrial Beta zeolite.
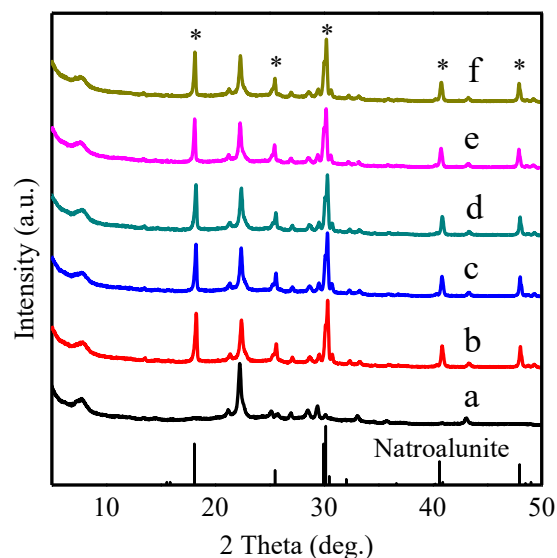
Fig. S2 XRD patterns of the Na Beta (a) and resultant CD Beta prepared with different mass of ethanol: 0 g (b), 0.25 g (c), 0.5 g (d), 0.75 g (e), and 1 g (f). The asterisks (*) indicate the diffractions attributed to natroalunite. Other treatment conditions, 1 g Na Beta : 0.695 g $Al_2(SO_4)_3 \cdot 18 H_2O$: x g ethanol : 1.46 g H_2O; temp., 423 K; time, 6 h.

The influence of ethanol on Al-rich Na-type Beta dealumination process was explored. The XRD patterns explicitly verify that parent Na Beta and the corresponding treated samples possess the BEA* topology. Besides the diffraction peaks due to Beta zeolite, those attributable to the natroalunite phase are also observed in the patterns of CD Beta. Unlike the CD process of NaY (Si/Al=2.4) in our previous published work where EtOH/H_2O medium decreased the dealumination rate and reduced the damage of the FAU framework [15], the peak intensity of both Beta and natroalunite phase were comparable despite the vibration of ethanol amount, indicating that the addition of ethanol in the process of $Al_2(SO_4)_3$ dealumination hardly effected the crystallinity, probably due to the higher Si/Al ratio of Na Beta (Si/Al=4.3) than NaY.
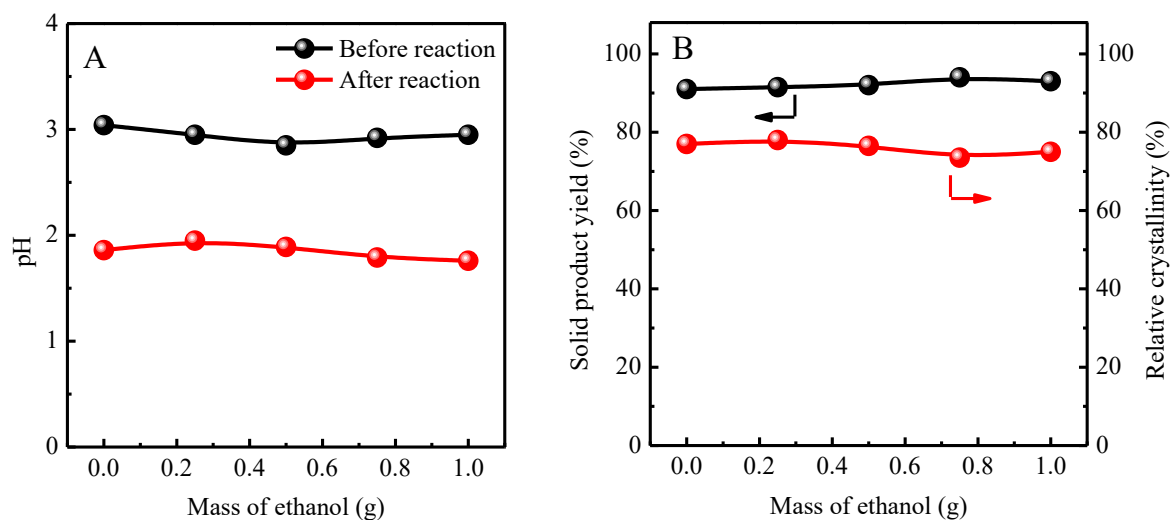
Fig. S3 pH value change in aqueous solution (A), solid product yield and relative crystallinity (B) of the Na Beta and resultant CD Beta with different mass of ethanol. Other treatment condition, 1 g Na Beta : 0.695 g $Al_2(SO_4)_3 \cdot 18\ H_2O$: x g ethanol : 1.46 g H_2O; temp., 423 K; time, 6 h.

Fig. S3A investigated the pH value change of $Al_2(SO_4)_3$ solution before and after the dealumination process with different ethanol amounts. The generation of natroalunite ($NaAl_3(SO_4)_2(OH)_6$) consumes the OH^- ions in the solution and reduced the pH value. The pH values decreased from about 3.1 to about 1.9 in all the $Al_2(SO_4)_3$ solutions with different ethanol amounts. The solid product yield and relative crystallinity of all CD Beta samples were also similar and about 90% and 78%, respectively (Fig. S3B). On the whole, the ethanol was not necessary for the dealumination of Na Beta.
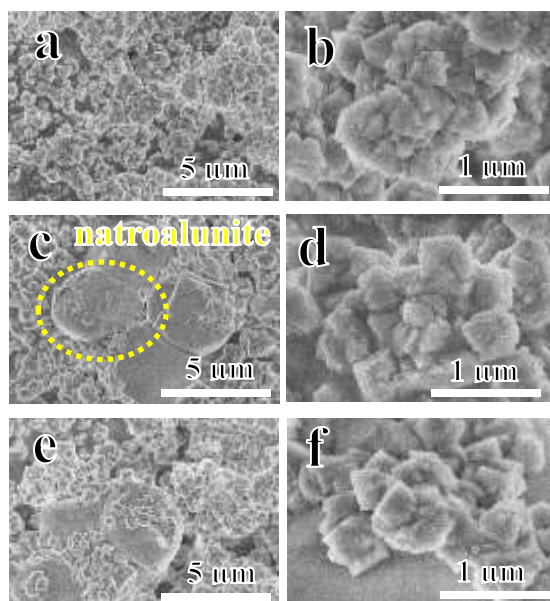
Fig. S4 SEM images of the Na Beta (a, b) and resultant CD Beta prepared with different mass of ethanol, 0 g (c, d) and 0.75 g (e, f). Other treatment condition, 1 g Na Beta : 0.695 g $Al_2(SO_4)_3 \cdot 18\ H_2O$: x g ethanol : 1.46 g H_2O; temp., 423 K; time, 6 h.

SEM images (a, b) of Na Beta show intergrown crystals with a truncated octahedral morphology and well-defined surfaces. After dealumination by $Al_2(SO_4)_3$ with different ethanol amounts (c-f), the morphology showed no obvious change, and natroalunite phase with rough ball-shaped crystals could be clearly seen.
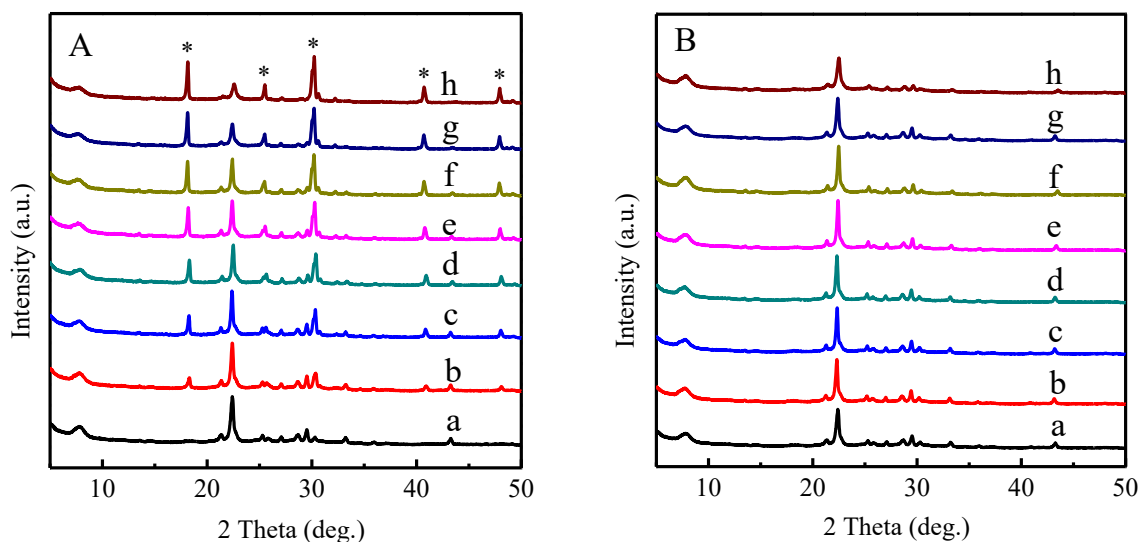
Fig. S5 XRD patterns of (A) CD Beta and (B) DeAl Beta prepared with a different $Al_2(SO_4)_3$ concentration of 0 M (a), 0.16 M (b), 0.32 M (c), 0.48 M (d), 0.64 M (e), 0.8 M (f), 1.12 M (g), and 1.44 M (h). The asterisks (*) indicate the diffractions attributed to natroalunite. Other treatment condition: 1 g Na Beta : x g $Al_2(SO_4)_3 \cdot 18\ H_2O$: 1.46 g H_2O; temp., 423 K; time, 6 h.

As shown in Fig. S5A, with the increase of $Al_2(SO_4)_3$ concentration, the diffractions of natroalunite became more intense, while the intensity of the reflection peaks attributed to Beta phase after selectively removing the natroalunite phase was gradually weakened, indicating that more natroalunite generated by extracting FAL.
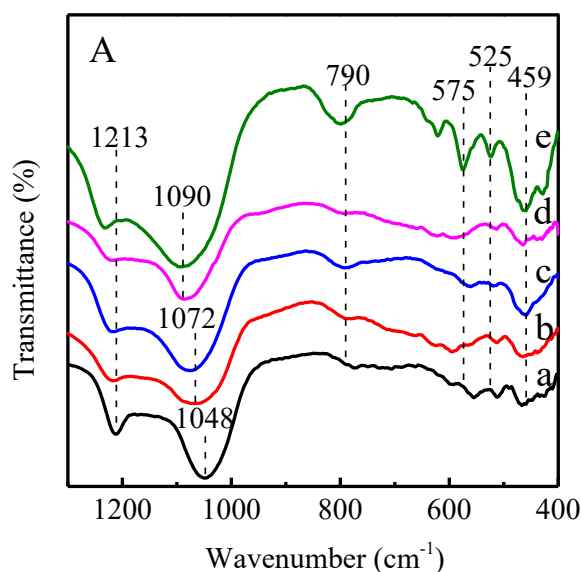
Fig. S6 FT-IR spectra (A) of Na Beta (a), CD Beta-7.6 (b), DeAl Beta-12 (c), CD Beta-7.6 (d), and DeAl Beta -12 (e).

After CD treatment, although the bulk Si/Al ratio decreased from 4.3 in Na Beta to 2.1 in CD Beta-7.6 and 1.9 in CD Beta-12, respectively, the band of asymmetric T–O–T stretching vibrations blue-shifted after CD process, indicating part of the FAL species in Na Beta were removed. The wavenumbers of these vibrations of DeAl Beta-7.6 (Fig. S6c) and DeAl Beta-12 (Fig. S6e) were comparable with those of corresponding CD Beta, meaning that the washing step did not affect the framework Si/Al ratio. The skeletal vibrations at 575, 525 and 459 cm^{-1} of CD Beta-7.6 (Fig. S6b) and CD Beta-12 (Fig. S6d) became weak because of the coexisting natroalunite compared with Na Beta (Fig. S6a), but these vibration bands of DeAl Beta-7.6 (Fig. S6c) and DeAl Beta-12 (Fig. S6e) were found to become more pronounced after removing natroalunite, stronger than that of Na Beta (Fig. S6a), characteristic of highly crystalline Beta zeolite.
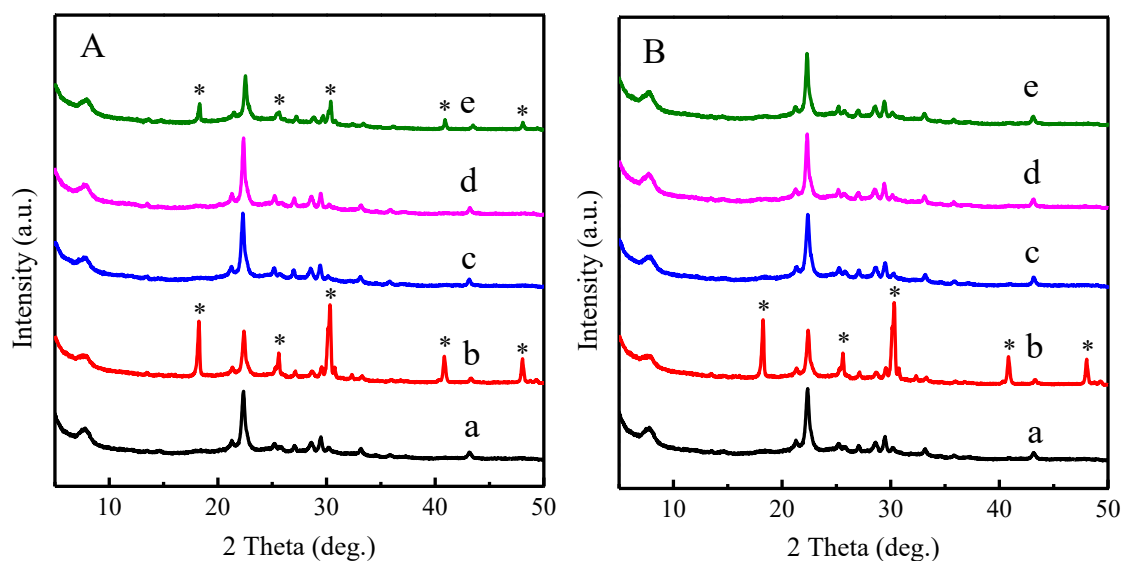
Fig. S7 XRD patterns (A) of Na Beta (a) and $Al_2(SO_4)_3$ (b), $AlCl_3$ (c), $Al(NO_3)_3$ (d) treated Na Beta samples with the same Al^{3+} content, or H_2SO_4 (e) treated Na Beta samples with the same SO_4^{2-} concentration with $Al_2(SO_4)_3$. XRD patterns (B) of Na Beta (a) and $Al_2(SO_4)_3$ (b), $AlCl_3$ (c), $Al(NO_3)_3$ (d), H_2SO_4 (e) treated Na Beta samples with the same pH condition. The asterisks (*) indicate the diffractions attributed to natroalunite. Other treatment condition: 1 g Na Beta : x g Al salts or H_2SO_4 : 1.46 g H_2O; temp., 423 K; time, 6 h.

When Na Beta was treated by $Al_2(SO_4)_3$ at pH of 3.1, natroalunite was formed, and the framework Si/Al ratio increased from 4.3 for Na Beta to 7.6 for CD Beta. When the treatment was conducted using $AlCl_3$, $Al(NO_3)_3$ with the same Al^{3+} or H_2SO_4 with same SO_4^{2-} of $Al_2(SO_4)_3$ (Fig. S7A), no crystalline natroalunite phase was formed except for the case treated by H_2SO_4 solution. The strong sulfuric acid extracted a small amount of framework Al and Na atoms and reacted with SO_4^{2-} to form limited amount of natroalunite phase, and the framework Si/Al ratio of the resultant Beta zeolites remained in a low value of 4.9, indicating negligible dealumination. Moreover, there was no natroalunite phase when using $AlCl_3$, $Al(NO_3)_3$ and H_2SO_4 under the same pH of 3.1 (Fig. S7B), mainly because natroalunite could not be formed without the simultaneous presence of SO_4^{2-} and Al^{3+} in the aqueous solution. Thus, the formation of natroalunite was critical to realize cannibalistic dealumination using Al sources.
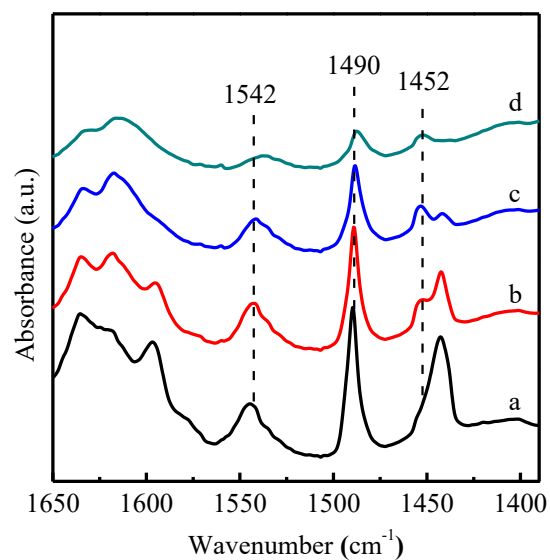
Fig. S8 FT-IR spectra of CD-Beta-7.6 after pyridine adsorption and desorption at different temperatures of 323K (a), 423K (b), 523K (c), 623K (d).

As shown by the pyridine-adsorbed IR spectroscopy, the obvious band at 1542 cm^{-1} of CD Beta-7.6 revealed the presence of Brønsted acid sites in proton type Beta zeolite.
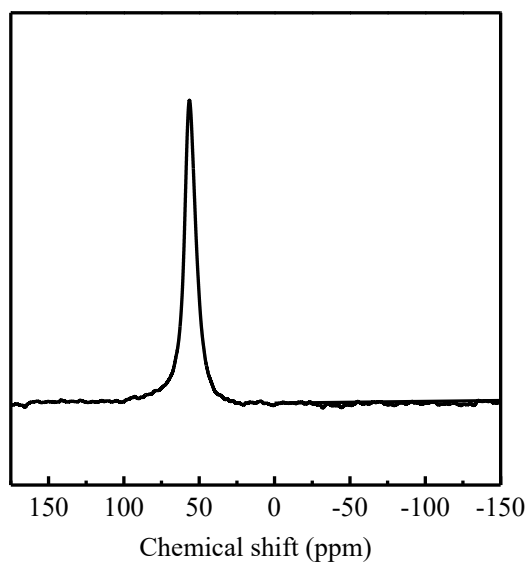
Fig. S9 ^{27}Al MAS NMR spectrum of the DeAl Beta-7.6 after calcination at 823 K for 6 h.

The DeAl Beta-7.6 after calcination exhibited a resonance at ~57 ppm in the ^{27}Al MAS NMR spectrum, which is typically assigned to tetrahedrally coordinated aluminum in zeolite framework, and there was no resonance ascribed to octahedral coordinated extra-framework aluminum species between 0 and 3 ppm [17], indicating stable structure of DeAl Beta-12 after CD process.
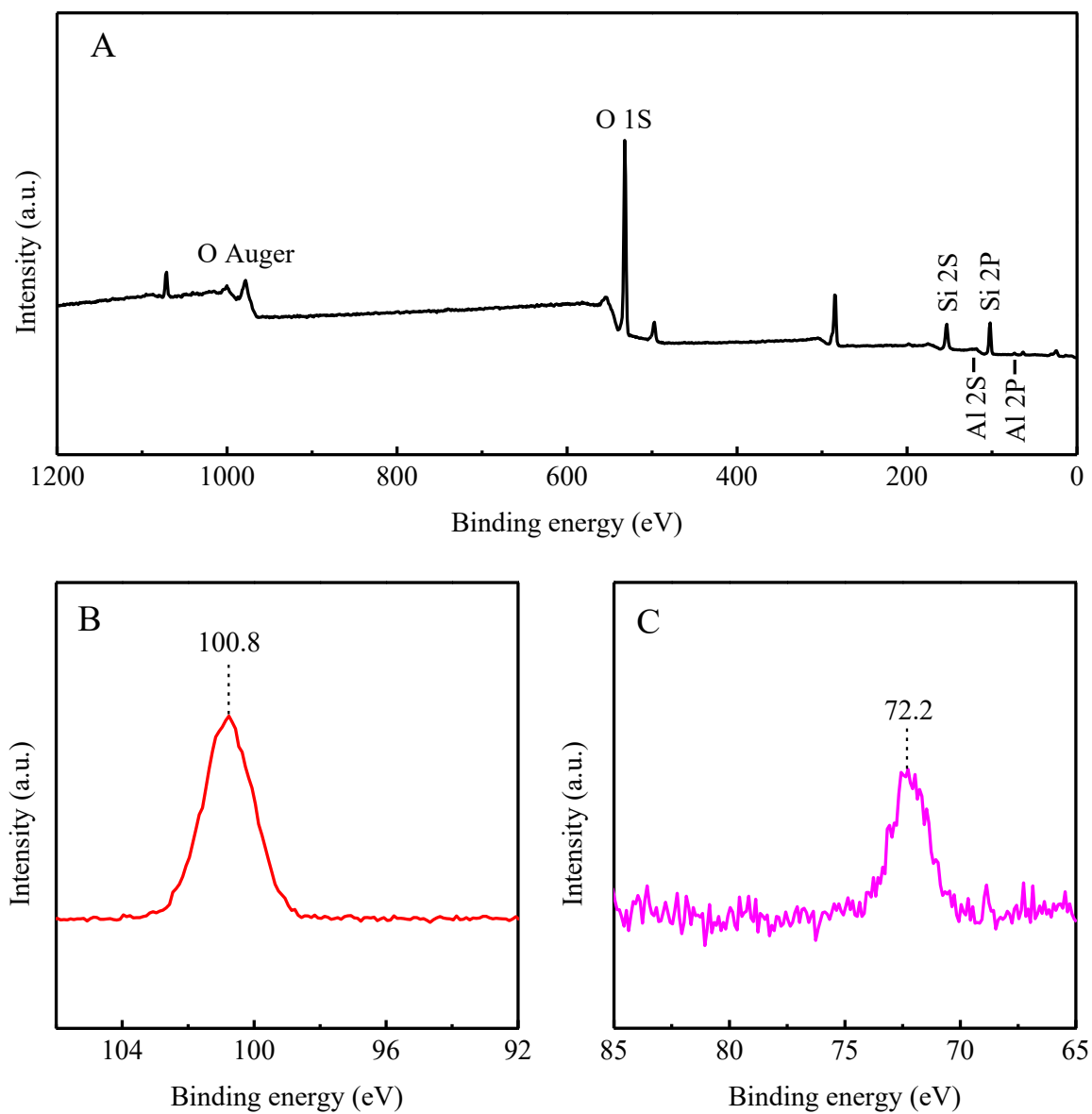
**Fig. S10** Whole XPS spectrum (A), Si 2p XPS spectrum (B) and Al 2p XPS spectrum (C) of industrial Beta.

XPS spectrum can reveal the external surface composition of zeolite [18-20]. The calculated Si/Al ratio by XPS spectrum on the surface of industrial Beta was 5.1.
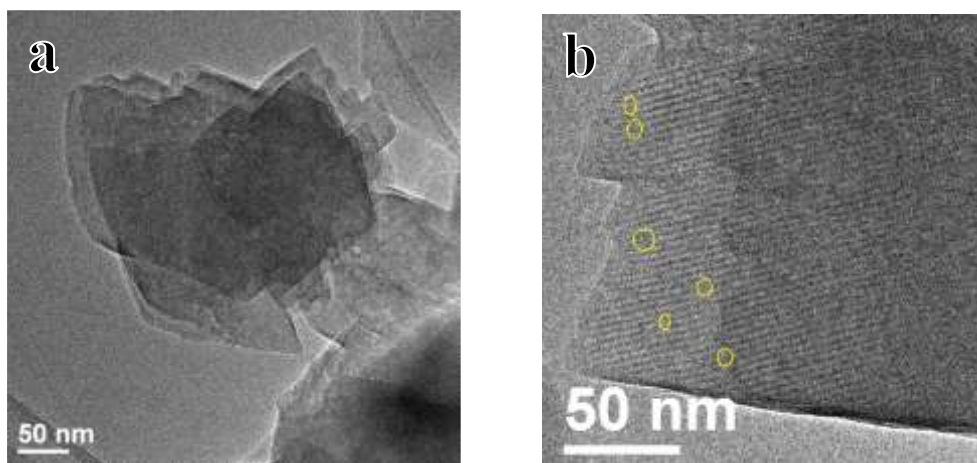
Fig. S11 TEM images of DeAl Beta -12.

Obvious bright spots were observed in the DeAl Beta-12 zeolite after the dealumination process, indicating that large amount of FAL was extracted by $Al_2(SO_4)_3$ (Fig. S10a). As shown in Fig. S10b, the characteristic crystal lattice fringes and intracrystal mesoporous (holes, yellow circle) could be observed for DeAl Beta-12 zeolite within the same crystal, verifying that the crystalline structure of Beta zeolite crystals was well maintained and mesopores were created by dealumination.
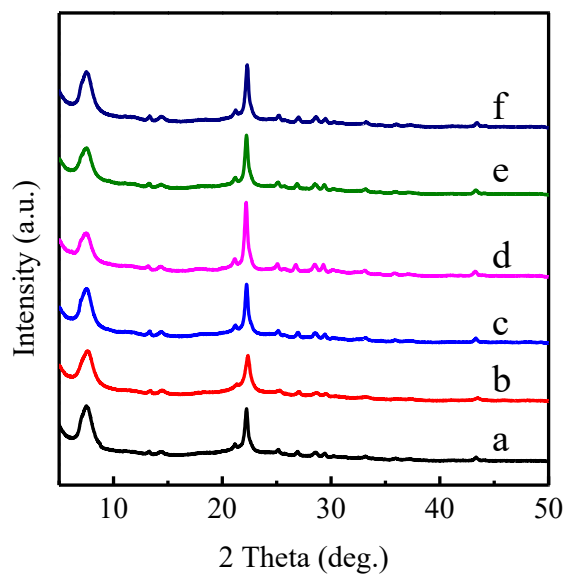
Fig. S12 XRD patterns of PR Beta (a), PR Beta after hydrothermal stability test (b), DeAl Beta-7.6 (c), DeAl Beta-7.6 after hydrothermal stability test (d), DeAl Beta-12 (e) and DeAl Beta-12 after hydrothermal stability test (f).

As shown by XRD patterns after hydrothermal stability test, there was no decrease in intensity for DeAl Beta-7.6 and DeAl Beta-12 and their relative crystallinity were 104% and 109%, respectively compared with the parent DeAl Beta, indicating that the BEA* topology was totally preserved (Fig. S11, b and c), but the intensity of PR Beta with a lower Si/Al ratio obviously decreased after steaming (relative crystallinity was 85%), indicative of a relatively poor hydrothermal stability (Fig. S11a).
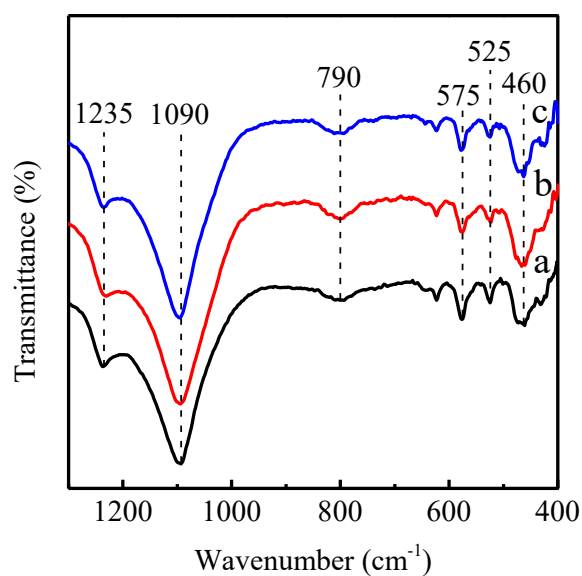
Fig. S13 FT-IR spectra of PR Beta (a), DeAl Beta-7.6 (b), and DeAl Beta-12 (c) after hydrothermal stability test.

It can be seen from the vibrations of fingerprint region of FT-IR spectra that the structural units of BEA* topology were well maintained in hydrothermal test. Meanwhile, the asymmetric T-O-T stretching vibration has moved to higher wavenumbers, especially for PR Beta (from 1048 to 1090 cm^{-1}), indicating that further dealumination of Beta zeolites occurred during the hydrothermal treatment.
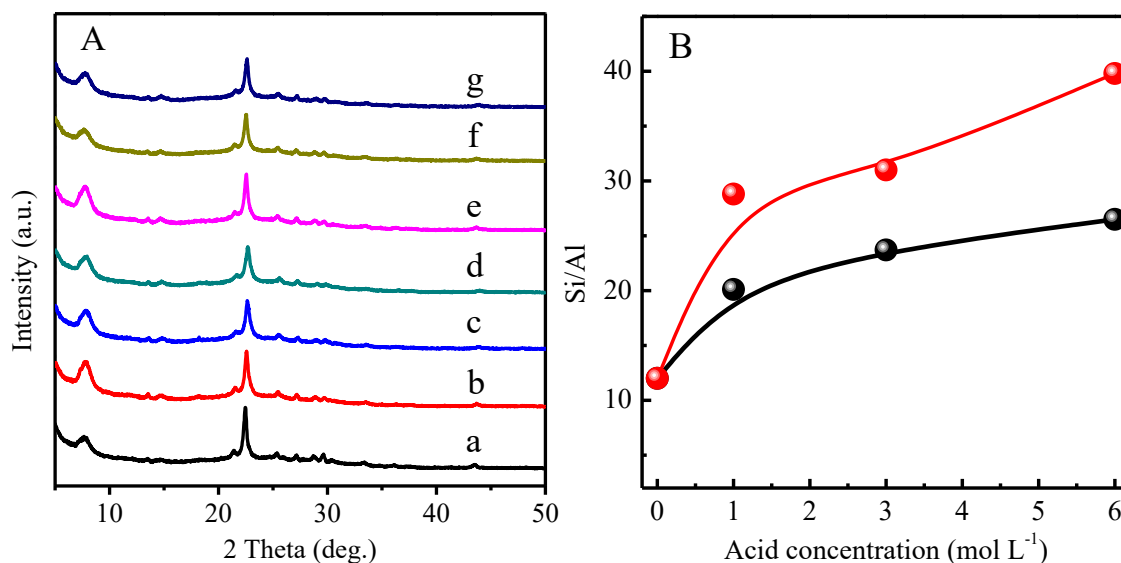
Fig. S14 XRD patterns (A) of DeAl Beta-12 (a) and further dealumination of DeAl Beta-12 zeolites with different concentrations of HNO_3 solution at ambient temperature (293 K): 1 M HNO_3 (b), 3 M HNO_3 (c), 6 M HNO_3 (d); or under 413 K reflux condition: 1 M HNO_3 (e), 3 M HNO_3 (f), 6 M HNO_3 (g). Si/Al ratios (B) of the further dealumination zeolites as a function of acid concentration in ambient temperature (black line) or under 413 K reflux condition (red line). Other further dealumination conditions: l/s (mass)= 20; treating time, 2 h.

DeAl Beta-12 was further dealuminated by acid leaching with an aqueous HNO_3 solution for 2 hours at ambient temperature (293 K) or under 413 K reflux condition, and the HNO_3 concentrations used were 1 M, 3 M, and 6 M, respectively. It was reported that the structure of Al-rich Beta zeolite (Si/Al=5) completely collapsed upon strong mineral acid treatment, which resulted in the formation of high lattice defect concentrations and diminished the stability of the crystal structure [21]. In contrast, the Beta structure almost remained intact after the CD process followed by the acid treatments (Fig. S14A), suggesting the pre-dealumination by $Al_2(SO_4)_3$ could stabilize Beta structure. Further acid leaching drastically increased the Si/Al ratio from 12 to 39 by further removal of Al atoms from zeolite framework (Fig. S14B). Thus, the Al-rich Beta can be efficiently dealuminated by $Al_2(SO_4)_3$ followed by the acid leaching, giving tunable Si/Al ratios.
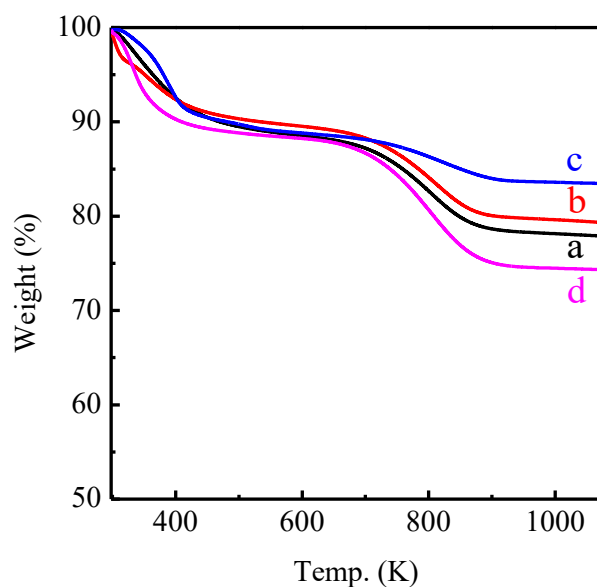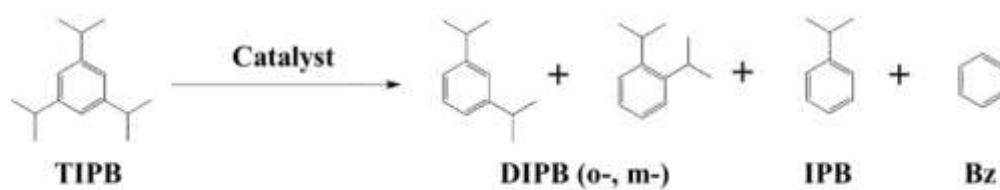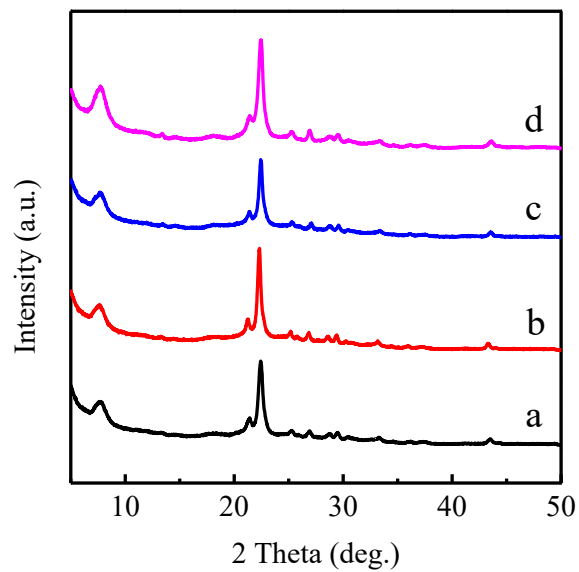
Fig. S15 TG curves of used PR Beta (a), DeAl Beta-7.6 (b), and DeAl Beta-12 (c), and industrial Beta (d) after the TIPB cracking reaction for 3 h.

TG curves of samples showed two weight losses. The one before 473 K can be attributed to the physically adsorbed water, while weight losses in the range of 673 - 873 K can be assigned to the coke [23,24]. The results showed that the coke amount of PR Beta (Fig. S15a) reached up to 10.3 wt%, which indicated that the relatively small micropores in Beta zeolites significantly affected the mass transport in catalytic reaction, resulting in severely coke formation and deactivation of catalyst. A lower amount of carbon deposition (9.2 wt%) was observed for DeAl Beta-7.6 (Fig. S15b) after CD process. With further dealumination, DeAl Beta-12(Fig. S15c) showed a much lower carbon deposition, only 4.3 wt%, mainly due to its hierarchical pore system (Fig. 7Ae) and less acid sites than PR Beta. However, the industrial Beta (Fig. S15d) had the highest carbon deposition (13.4 wt%), probably due to nanosized crystals and Al-rich surface, resulting in the highest initial activity and fastest coke deposition rate.

Fig. S16 Reaction scheme of TIPB cracking (showing only main products). Reaction conditions: temp., 573 K; cat., 0.2 g; WHSV, 7.2 h^{-1}.

The cracking of TIPB was a successive reaction with the main products of diisopropylbenzene (DIPB) isomers, isopropylbenzene (IPB), and benzene (BZ), and the product distribution provided information concerning the extent of cracking degree. The stronger the catalytic capacity of the catalyst, the more products of deeper cracking [22, 23].

Fig. S17 XRD patterns of used PR Beta (a), DeAl Beta-7.6 (b), DeAl Beta-12 (c), and industrial Beta (d) after the TIPB cracking reaction for 3 hours.

The catalysts after the TIPB cracking reaction were analyzed by XRD. Despite the presence of coke deposition after the reaction, the structure of the four catalysts showed high crystallinity.
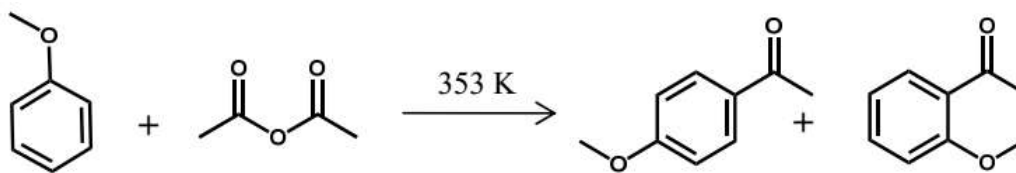
Fig. S18 Reaction scheme of acylation of anisole with acetic anhydride. Reaction conditions: temp., 353 K; cat., 0.1 g; anisole, 5.23 g; acetic anhydride, 5 mmol.

In the Friedel-Crafts acylation of anisole with acetic anhydride reaction, the p-methoxyacetophenone (p-MAP) was the main product with the selectivity over 98% [25, 26].

References

1 R. Otomo and T. Yokoi, Effect of the Al Content in the Precursor on the Crystallization of OSDA-Free Beta Zeolite, Microporous Mesoporous Mater., 2016, **224**, 155-162.

2 A. La Iglesia and A. J. Aznar, A Method of Estimating the Gibbs Energies of Formation of Zeolites, Zeolites, 1986, **6**, 26-29.

3 S. J. L. G. C. Gang, A New Method of Calculating Gibbs Free Energy of Formation of zeolites, J. Chem. Ind. Eng., 2006, **57**, 2806-2811.

4 S. Gaboreau and P. Vieillard, Prediction of Gibbs Free Energies of Formation of Minerals of the Alunite Supergroup, Geochim. Cosmochim. Ac., 2004, **68**, 3307-3316.

5 W. M. Haynes and D. R. Lide, CRC Handbook of Chemistry and Physics, 2010, **p5**, 4-24.

6 G. Huang, P. Ji, H. Xu, J. Jiang, L. Chen and P. Wu, Fast Synthesis of Hierarchical Beta Zeolites with Uniform Nanocrystals from Layered Silicate Precursor, Microporous Mesoporous Mater., 2017, **248**, 30-39.

7 B. J. Schoeman, E. Babouchkina, S. Mintova, V. P. Valtchev and J. Sterte, The Synthesis of Discrete Colloidal Crystals of Zeolite Beta and Their Application in the Preparation of Thin Microporous Films, J. Porous Mater., 2001, **8**, 13–22.

8 Y. Liu, W. Zhang and T. J. Pinnavaia, Steam-Stable MSU-S Aluminosilicate Mesostructures Assembled from Zeolite ZSM-5 and Zeolite Beta Seeds, Angew. Chem. Int. Ed., 2001, **40**, 1225-1258.

9 A. D. Hadigavabar, K. Tabatabaeian, M. A. Zanjanchi and M. Mamaghani, Molybdenum Anchored onto Zeolite Beta: An Efficient Catalyst for the One-Pot Synthesis of Octahydroquinazolinone Derivatives under Solvent-Free Conditions, Reac. Kinet. Mech. Cat., 2018, **124**, 857–871.

10 E. Astorino, J. B. Peri, R. J. Willey and G. Busca, Spectroscopic Characterization of Silicalite-1 and Titanium Silicalite-1, J. Catal., 1995, **157**, 482–500.

11 A. Zecchina, S. Bordiga, G. Spoto, L. Marchese, G. Petrini, G. Leofanti and M. Padoan, Silicalite Characterization. 2. IR Spectroscopy of the Interaction of Carbon Monoxide with Internal and External Hydroxyl Groups, J. Phys. Chem., 1992, **96**, 4991–4997.

12 L. M. Kustov, V. B. Kazansky, S. Beran, L. Kubelkova, P. Jiru, Adsorption of Carbon Monoxide on ZSM-5 Zeolites. Infrared Spectroscopic Study and Quantum-Chemical Calculations, J. Phys. Chem., 1987, **91**, 5247–5251.

13 A. Simon-Masseron, J. Marques, J. Lopes, F. R. Ribeiro, I. Gener, M. Guisnet, Influence of the Si/Al Ratio and Crystal Size on the Acidity and Activity of HBEA Zeolite, Appl. Catal. A-Gen., 2007, **316**, 75-82.

14 I. Kiricsi, C. Flego, G. Pazzuconi, W. O. J. Parker, R. Millini, C. Perego, G. Bellussi, Progress toward Understanding Zeolite Beta Acidity: An IR and 27Al NMR Spectroscopic Study, J. Phys. Chem., 1994, **98**, 4627-4634.

15 Z. Shi, P. Ji, Z. Zhu, J. Jiang, W. Fu, P. Wu, Y. Wang and M. He, Stabilizing Low-Silica Zeolites through Aluminum Sulfate Assisted Cannibalistic Dealumination, ChemCatChem, 2016, **8**, 1891-1895.

16 S. Li, A. Zheng, Y. Su, H. Zhang, L. Chen, J. Yang, C. Ye and F. Deng, Brønsted/Lewis Acid Synergy in Dealuminated HY Zeolite: A Combined Solid-State NMR and Theoretical Calculation Study, J. Am. Chem. Soc., 2007, **129**, 11161-11171.

17 R. Bertram, U. Lohse and W. Gessner, Zur Charakterisierung des Extragitter-Aluminiums in Y-Zeolithen Mittels der Ferronmethode, Z. Anorg. Allg. Chem., 1988, **567**, 145-152.

18 H. Shimada, N. Matsubayashi, M. Imamura, T. Sato and A. Nishijima, Determination of External Surface Composition of Zeolite Particles by Synchrotron Radiation XPS, Catal. Lett., 1996, **39**, 125-128.

19 O. Gijzeman, A. Mens, J. H. Lenthe, W. J. Mortier and B. M. Weckhuysen, The Effect of Chemical Composition and Structure on XPS Binding Energies in Zeolites, J. Phys. Chem. B, 2003, **107**, 678-684.

20 L. Xu, D. Huang, C. Li, X. Ji, S. Jin, Z. Feng, F. Xia, X. Li, F. Fan, C. Li, P. Wu, Construction of Unique Six-Coordinated Titanium Species with an Organic Ligand in Titanosilicate and Their Unprecedented High Efficiency for Alkenes Epoxidation, Chem. Comm., 2015, **51**, 9010-9013.

21 Y. Wang, R. Otomo, T. Tatsumi and T. Yokoi, Dealumination of Organic Structure-Directing Agent (OSDA) Free Beta Zeolite for Enhancing Its Catalytic Performance in *n*-Hexane Cracking, Microporous Mesoporous Mater., 2016, **220**, 275-281.

22 X. Ji, H. Xu, D. Wang, L. Xu, P. Ji, H. Wu and P. Wu, Mesoporous MCM-22 Zeolites Prepared through Organic Amine-Assisted Reversible Structural Change and Protective Desilication for Catalysis of Bulky Molecules, ACS Catal., 2013, **3**, 1892-1901.

23 H. Liu, T. Li, B. Tian and Y. Xu, Study of Coke Deposition on Mo/HZSM-5 Catalyst in Methane Dehydro-Aromatization under Non-oxidative Conditions, Chin. J. Catal., 2001, **22**, 373-376.

24 C. Li and P. C. Stair, Ultraviolet Raman Spectroscopy Characterization of Coke Formation in Zeolites, Catal. Today, 1997, **33**, 353-360.

25 L. Xu, X. Ji, S. Li, Z. Zhou, X. Du, J. Sun, F. Deng, S. Che and P. Wu, Self-Assembly of Cetyltrimethylammonium Bromide and Lamellar Zeolite Precursor for the Preparation of Hierarchical MWW Zeolite, Chem. Mater., 2016, **28**, 4512-4521.

26 M. Guidotti, C. Canaff, J. M. Coustard, P. Magnoux and M. Guisnet, Acetylation of Aromatic Compounds over H-BEA Zeolite: The Influence of the Substituents on the Reactivity and on the Catalyst Stability, J. Catal., 2005, **230**, 375−383.